Separating Flow Over Repeated Surface-Mounted Ribs in a Square Duct

Shou-Shing Hsieh* and Ying-Jong Hong†
National Sun Yat-Sen University, Kaohsiung, Taiwan, Republic of China

Flow visualization, manometry, and hot-wire anemometry have been applied to approximately three-dimensional airflow around separated ribs with rib spacing-to-height ratio equal to 5.31, rib height-to-hydraulic ratio diameter 0.19, and Reynolds number ranging from 13,000 to 130,000 in order to simulate important aspects relating to turbine blade internal cooling design. Moreover, smoke flow pattern was observed and discussed in the range of $100 < Re_H < 9000$. The main features of the flow, which is eventually periodic in the streamwise direction, developing lengths, pressure loss coefficient, and mean and rms velocity distribution are presented.

Nomenclature

b	= distance between any pair of ribs, cm
D_H	= hydraulic diameter of the duct, cm
E	= voltage, V
e	= roughness height, cm
f	= friction factor
p	= pitch of two consecutive roughness elements, cm
Δp	= pressure drop, mm alcohol
Re_H	= Reynolds number based on hydraulic diameter, VD_H/v
u	= x-component mean velocity, m/s
u'	= x-component fluctuating velocity, m/s
V	= average velocity, m/s
u_m, $\bar{u}_m$	= average velocity and grand average velocity in a pitch, m/s
x	= downstream distance, cm
w	= width of ribs, cm
α	= rib angle, deg
v	= kinematic viscosity of air, m^2/s
ω	= frequency, Hz

Subscripts

e	= rib height
H	= hydraulic
p	= pitch
r	= reattachment
s	= separation

Introduction

THIS work is concerned with an improved roughness geometry for application to single-phase fluids in turbulent duct flow. The roughness type adopted for the present study is a two-dimensional repeated rib on the top ceiling and floor of the duct in a staggered alignment. Roughness is of great interest because it provides a substantial heat-transfer coefficient increase.[1-4] When this methodology is applied to turbine blade internal cooling design, repeated ribs may be used to minimize heat-transfer surface area for the same heat duty or increase the hot gas outlet temperature from the combustor.

Because the increase in heat-transfer rate performance is accompanied by a friction factor increase,[5,6] the preferred roughness geometry will yield a given heat-transfer augmentation with minimum friction factor rise. Many studies[7-11] have been conducted on transverse-rib roughness (90-deg helical angle). In some applications, such as gas turbine blade cooling design, the heat-transfer enhancement is required on two opposite walls of the cooling passages in order to remove more

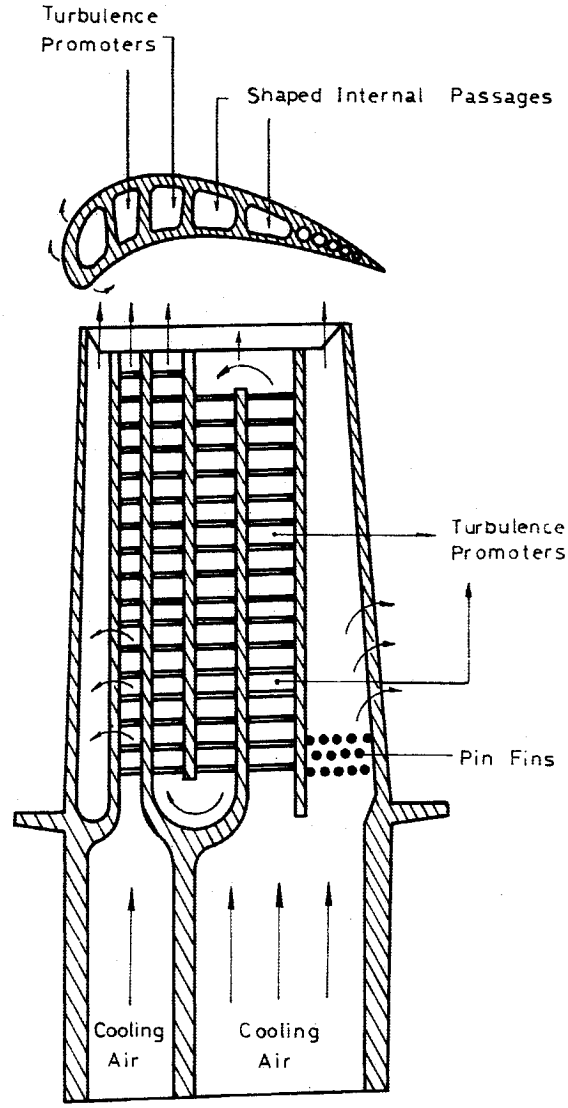

Fig. 1 Cooling concept of a modern multipass turbine blade.

Received June 29, 1987.

*Associate Professor, Department of Mechanical Engineering. Member AIAA.

†Graduate Student, Department of Mechanical Engineering.

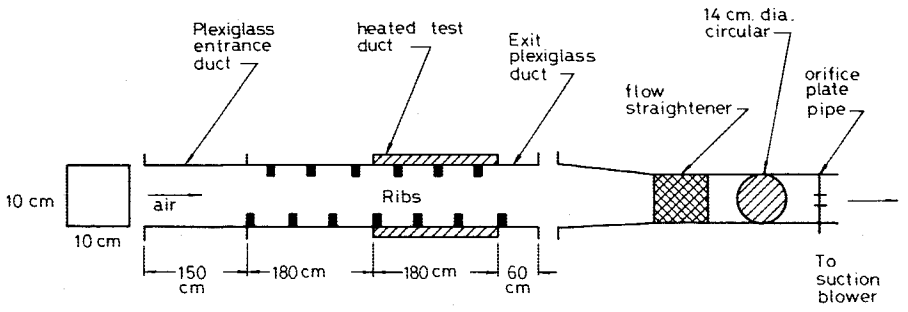

Fig. 2 Schematic of present repeated-rib duct with staggered-type alignment.

heat transferred from blade external surfaces, which are directly exposed to the hot gas flow. The current advanced gas turbine blade cooling system is as sketched in Fig. 1, and the turbulence promoters (i.e., repeated ribs) with a 90-deg angle to the flow have been cast onto the two opposite walls of the shaped internal passages.[12,13] The internal passages can be modeled approximately as that in the flow in rectangular channels with two opposite rib-roughened walls. The heat-transfer and friction characteristics in channels of this kind may be different from those of circular tubes, parallel plates, or annuli. The earliest experimental data were reported by Burggarff,[14] who studied the turbulent airflow in a square duct with two opposite ribbed walls with $\alpha = 90$ deg, $p/e = 10$, and $e/D = 0.55$. The results indicated that the augmentation of the Nusselt number on the ribbed side walls and on the smooth side wall was 138 and 19%, respectively, higher than the four-sided smooth duct flow values, whereas the friction factor was about 8.6 times higher. In this study, the emphasis was placed on the effect of the entrance conditions. Only one particular rib geometry ($\alpha = 90$, $p/e = 10$, $e/D = 0.055$) was tested. Later, Han and Lei[15] systematically investigated the effects of rib pitch-to-height and height-to-hydraulic diameter ratios on the friction factor and heat-transfer coefficients for fully developed turbulent airflow in a square duct with two opposite rib-roughened walls. The p/e ratio was varied from 10 to 40, and the e/D ratio was varied from 0.001 to 0.063, but the α was kept at a constant value of 90 deg. Based on the four-sided smooth duct correlation and the four-sided ribbed duct similarity law, a general prediction method for average friction Stanton number in rectangular channels with two opposite ribbed walls with $\alpha = 90$ deg was developed. Recently, Han et al.[16] re-examined the same work with different rib angles of attack on the pressure drop and the average heat-transfer coefficients in the fully developed turbulent air flow. The thermal performance comparison indicated that the increased heat conductance for the rib with an oblique angle to the flow ($\alpha = 45$–30 deg) was about 10–20% higher that the rib with a 90-deg angle to the flow, and the pumping power requirement for the angled rib was about 20–50% lower than the transverse rib.

The papers previously cited focused on the area of heat-transfer enhancement. For flow pattern and basic fluid dynamics behaviors, several papers have been studied.[17-19] Most recently, Stukel et al.[20] and Nourmohammadi et al.[21] have investigated in detail turbulent airflow over rough surfaces (repeated ribs) on both mean flow parameter and turbulent flow parameters with $p/e > 10$. In light of the foregoing discussions, it appears that there is a need for a study of turbulent airflow in a square duct with two opposite ribbed walls in staggered-type alignments and with $p/e < 10$. Moreover, a flow visualization will be made to provide more insight regarding this complex physical process for low Reynolds numbers, $100 < Re_H < 9000$. This paper will investigate air channel flow around separated ribs with rib spacing-to-height ratio equal to 5.31, rib height-to-hydraulic diameter ratio 0.19, and Reynolds number ranging from $13{,}000 < Re_H < 130{,}000$ based on flow visualization, manometry, and hot-wire anemometry techniques to define flow characteristics on this kind of rough surface.

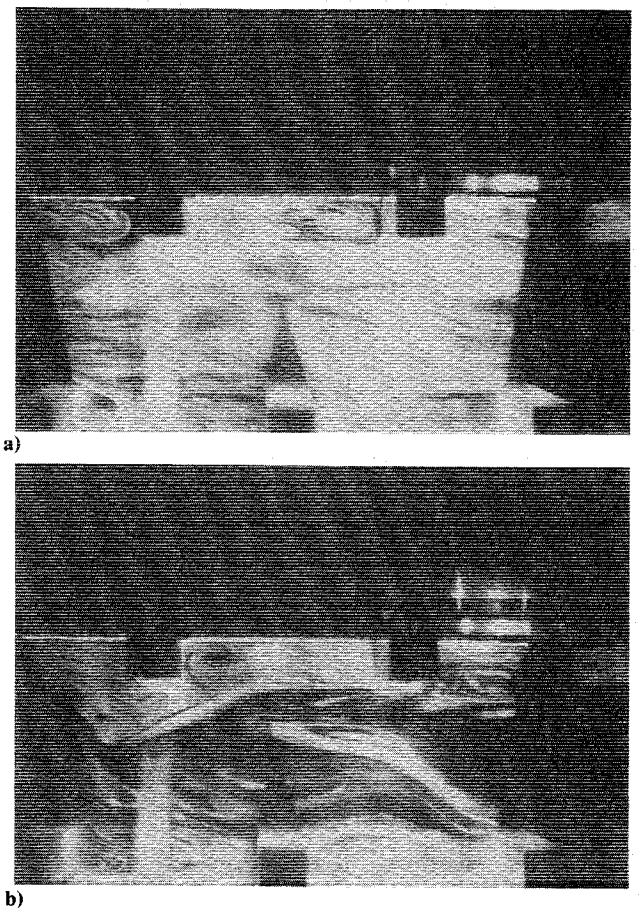

a)

b)

Fig. 3 Flow pattern over repeated ribs with staggered-type configuration with a) $Re_H = 2019$ and b) $Re_H = 6520$.

Experimental Apparatus and Procedure

A schematic of the air duct, which is 10 cm wide and 10 cm high, is shown in Fig. 2. Entering the inlet of the duct with a uniform velocity profile, the flow develops hydrodynamically in an unheated region before entering a 360-cm-long roughened test section. To facilitate flow visualization technique, all sections of the channel were constructed from 10-mm plexiglass. The roughness elements were made of aluminum rib, which was cemented to the ceiling and the floor of the duct oppositely in a staggered-type arrangement. A 3-hp suction blower drew air at room temperature and pressure through a 14-cm diam tube equipped with a 9.8-cm-diam circular orifice plate to measure flow rate. The blockage ratio for the rib height of 1.9 cm was 5%. For static pressure measurements, two static pressure tubes were placed at the center of channel to minimize the influence of velocity fluctuations. These static pressure measurements were used to find the friction factor f. A DISA 56C01 constant temperature hot-wire anemometer in conjunction with DISA 56N22 and 56N25 dc voltmeters was used to measure the turbulent mean flow characteristics and the velocity fluctuations.

The single DISA hot-wire probe consisted of 1.8-cm-long prongs (as height of the rib $e = 1.9$ cm, the stem of the probe never entered the valley between two consecutive ribs) made of hypodermic tubing of 1-mm diam; the spacing between the centers of the prongs was 2 mm. The stem was 33.8 cm long with 4-mm diam; it tapered down to 2-mm diam in the lower 2.2-cm position adjacent to the prongs. Thus, the blockage ratio of the prongs in the valley region was 1.2%, and that of the stem in the test section region was less than 5%. Our experience and previous investigations[22] have shown that with such low blockage ratios the interference to the flow is negligible. The sensor was made from Wollaston platinum wire of 7.5-μm diam. As the effective length of the sensor was 1 mm, the aspect ratio was about 125. In view of the low wind velocities, a comparatively low overheat value of 0.76 was employed. The normal orientation of the hot-wire axis was parallel to the rib edge from which the flow separated.

The hot-wire anemometry technique has some merits, e.g., fine space resolution of almost a point measurement, minimal sensor interference to the flow, fast frequency response for the intensity of fluctuations, and high-resolution electrical output. However, a single hot wire is insensitive to flow direction in pitch and therefore cannot detect the reverse velocity direction. For the same reason, mean streamwise velocity measurements are not very reliable near the corners, where the inclination of the mean flow streamlines to the valley floor is insignificant. Also, the hot-wire anemometer gives accurate values of the intensity of fluctuations only when the fluctuations are small compared to the mean velocity. But since the more sophisticated instrumentation such as the laser anemometer was not available to the authors and, more important, the detailed measurements of the mean velocity and intensity of fluctuations have not been reported previously in the literature of the present subject, it is hoped that the present results of the hot-wire measurements will be found valuable, at least for getting a picture of the qualitative trends. The problem of the shape of the calibration curve in the low-speed region was tackled in the following manner. The speed u was calculated by measuring the frequency ω of vortex shedding past a thin wire and using the empirical relation between ω and u given by Tritton.[23] The values of u so calculated were plotted against the voltage E, and a fourth-degree curve was fitted, using the least-square technique. However, since a single wire probe was used, there was no way to rectify the error due to inclination of the streamlines. Although we are aware that such an error becomes significant in the corner regions, this was a limitation of the present investigation.

The smoke flow visualization technique was employed to obtain the overall qualitative picture of the complicated, recirculating-type flow with corner regions, which are characteristic of separated flows over rectangular ribs. The location of reattachment was determined by projecting a 35-mm negative smoke pattern using a slide projector. The smoke was sucked into the test section through pressure taps located in the ceiling of the models, and the fore and aft motion of the smoke was observed.

The pressure drop across the test section was measured by a micromanometer and an inclined manometer. In fully developed duct flow, which is the case of the present configuration to be shown in Fig. 6, the friction factor can be determined by measuring the pressure drop across the flow channel and the mass flow rate of the air. The friction factor can be obtained from the Darcy-Weisbach formula for different flow rates. The flow rate can be measured by using an electronic differential manometer with a pressure cell of 0.015 kg/cm^2 range interfaced with an IBM personal computer in which the corresponding Reynolds number can be directly read out.

Results and Discussion

Flow Visualization

Before undertaking velocity measurements, flow visualization was conducted 1) to deduce the main features, and 2) to observe the dependence of the flow pattern, the onset of separation, and reattachment length. Typical photographic sequences are shown in Fig. 3 for low Reynolds numbers, $Re_H = 2019$ and 6520. In general, the results are comparable to those presented by Sinha et al.[22] One may observe vortices being shed periodically in the curved shear layer from the downstream sharp corner of the ribs as seen in Fig. 3. Slight differences in the patterns evolve as Reynolds numbers change. The flow in the recirculating regions between two consecutive ribs exhibits a definite pattern. It was characterized by two separation vortices, one formed due to the upstream face and the other formed due to the downstream face of the valley between two consecutive ribs. It appears that the separation point of these two vortices shifts further downstream as the Reynolds number increases.

Smoke flow visualization showed, in Fig. 4, that the separation and reattachment had occured under certain Reynolds numbers. The onset separation length and reattachment length are found to be nearly a linearly increasing function for low Reynolds numbers ($Re_H < 1500$), as shown in Fig. 5. This is in agreement with the tendency exhibited by the data of Sinha et

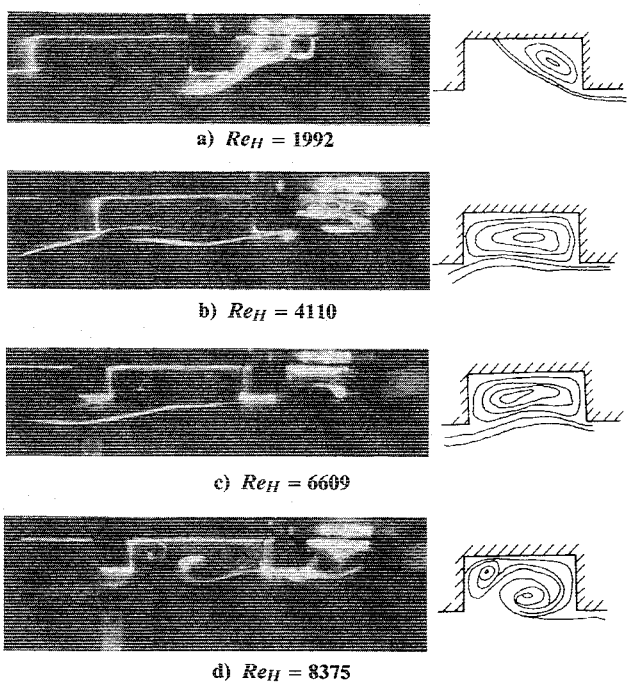

Fig. 4 Smoke patterns and schematic representation for flow over ribs.

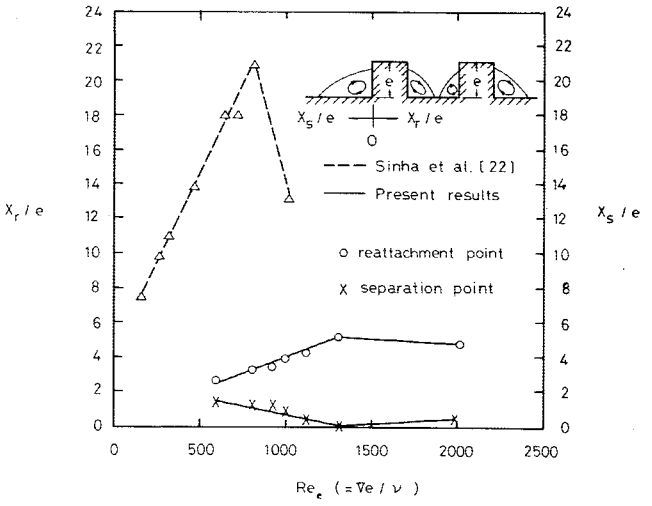

Fig. 5 Variation of reattachment and separation length with Reynolds number in the range of $100 < Re_e < 2000$.

al.[22] indicated by different types of broken line in Fig. 5. The maximum value of X_r observed in the present experiments was about five times the rib height at $Re_H = 1300$. On the contrary, the zero value of the onset of separation length of X_r was also observed at $Re_H = 1300$. The reattachment length (onset of separation length) starts decreasing (increasing) once the separating shear layer undergoes transition before reattachment (separation). This is observed in Fig. 5, where X_r/e and X_s/e vs Re_e plotted in the range of $100 < Re_H < 2000$. The discrepancy in magnitude was expected because of the different type of flow; one is external flow over an isolated (single) rib, and the other is internal flow with repeated ribs.

Static Pressure Measurements

The pressure drop was measured successively from ribs 1 to 35 for apparently turbulent flow. Reynolds numbers based on the cross section of the main channel ranged from 13,000 to 130,000. Figure 6 shows the fall of the static pressure along the test section in the axial direction at small holes (5 mm in diameter) in the ceiling of the test duct. Five positions (A–E) have been measured for the present study. For five different Reynolds numbers, the graph shows that the pressure gradient along the test section is constant, and the flow therefore is fully developed in a "spatially" periodic sense. The isothermal friction factor f is calculated based on $D'_H = D_H - 2e$. Table 1 summarizes these results for different Reynolds numbers. The experimental uncertainties calculated by the technique of Kline and McClintock[24] varied from 9–5% for f and 5–3% for Re as the Reynolds number was increased. The friction factor for turbulent, streamwise periodic flow is presented in Fig. 7. Friction factor f is approximately constant, which indicates the fully roughened regime of the flow under consideration.

Mean Velocity and Velocity Fluctuations

Generally speaking, the development of the mean velocity measurement at the centerplane is demonstrated in Fig. 8. Due to the present asymmetrical configuration in nature in one pitch, the maximum velocity does not coincide with the geometrical centerline of the duct. Consequently, the maximum velocity shift toward the side of the pair of ribs was observed. Such location shift could be attributed to the unbalanced shear forces caused by different surface conditions. By comparing the profiles between any pair of ribs, one can see that the general profile shapes are approximately the same at both flow rates. For both Reynolds numbers, $u(x)$ goes through zero at the same point. One might say the eye of the recirculation region appears to follow the same locus in both cases. Between the first pair of ribs, the mainstream flow is approximately uniform, as in an initial wall jet. The reversed flow region is weak relative to its later magnitude. The two regions accelerate in passing over the next several ribs, approaching profiles with sharper and higher peak values. The location of $u = 0$ moves slightly toward the downstream rib to a position slightly greater than $x/b = 1/5$. The number of ribs required for $u(x)$ to become spatially periodic within 1% was determined by comparing the data between successive ribs from Fig. 8. For $Re_H = 13{,}000$, flow must pass over five ribs, but only four for $Re_H = 130{,}000$. These observations also verified the findings of previous pressure-drop measurements. At the center of the duct, the mean axial velocity u was measured along the center axis at one flow rate. It is found that the centerline velocities were normalized by dividing by the velocity averaged over one pitch and the axial distance expressed as a percentage of the pitch length p, $X_p = (x/p)$, in order to compare the results with that of Ref. 20. This normalized velocity u_m/u_m is plotted against X_p in Fig. 9. It is found that, in

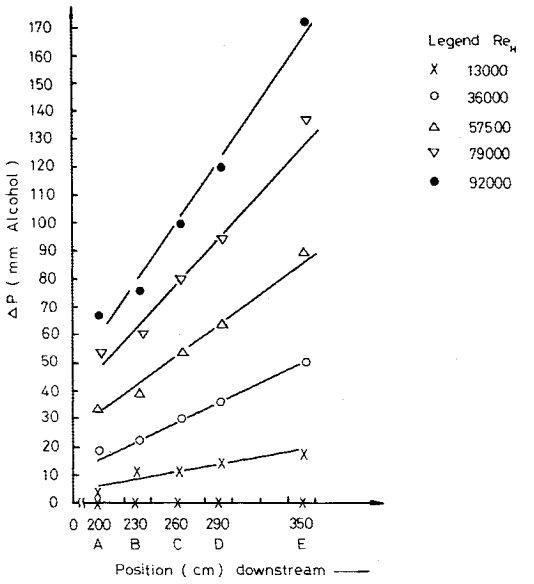

Fig. 6 Static pressure distribution along downstream distance.

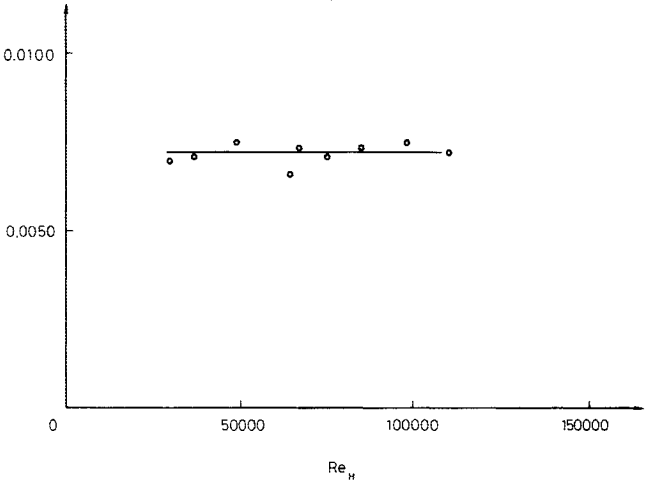

Fig. 7 Friction factor vs Re_H ($D'_H = D_H - 2e$).

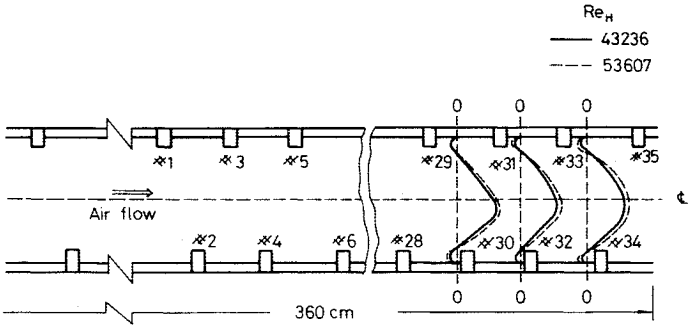

Fig. 8 Surface roughness element relative position and mean velocity distributions at downstream distance for $Re_H = 43{,}238$; 53,607.

Table 1 Values of friction factor varied with Reynolds number

Re_H	29,831	37,238	49,133	64,902	67,968	76,374	86,448	98,900	110,000
$f(D'_H = D_H - 2e)$	0.0070	0.0071	0.0075	0.0066	0.0073	0.0071	0.0073	0.0075	0.0072

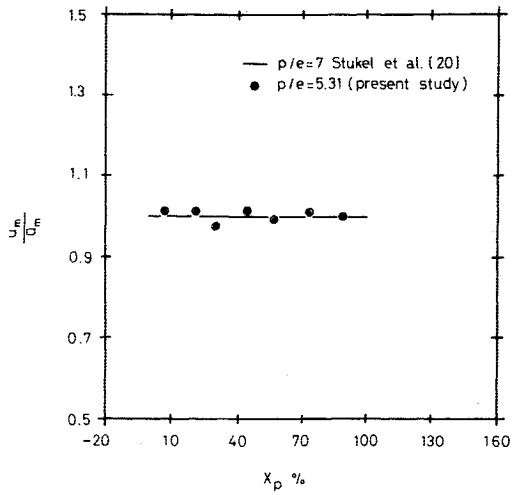

Fig. 9 Center of the pipe mean axial velocity as a function of the cycle length.

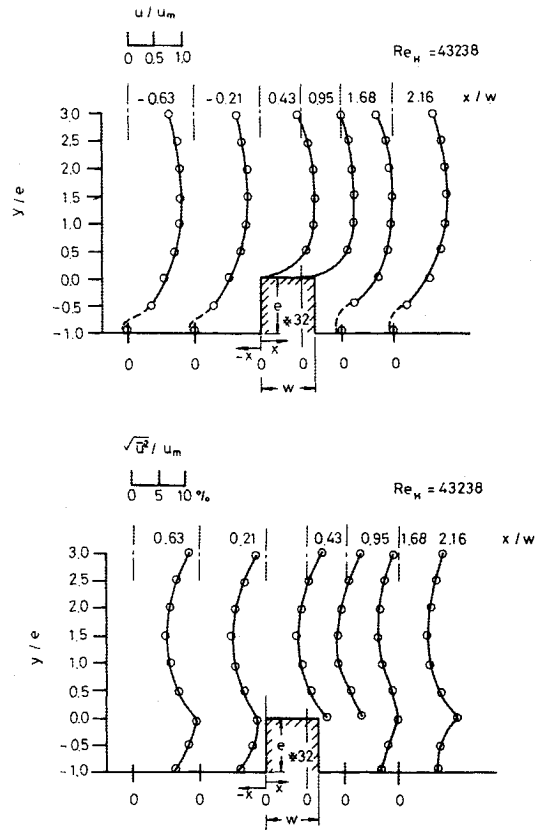

Fig. 10 Mean velocity and fluctuation intensity profiles for $Re_H = 43,283$ near a downstream rib.

spite of the present staggered-type arrangement, the variation of centerline velocity is consistent with that of Ref. 20.

To quantify flow development and downstream behavior in turbulent flow, mean velocity and velocity fluctuation were taken at $Re_H = 43,238$ and 53,607 for two different test regions, one near the rib, the other in the valley of two consecutive ribs. The typical development of mean velocity profile and intensity of fluctuations for these two cases are shown in Figs. 10, 11, 12, and 13, respectively. Following are the salient features of these profiles.

1) Near the rib, the mean velocity profiles shown in Figs. 10a and 11a have features similar to those predicted by Benodekar et al.[25] Slight differences due to different Reynolds numbers were found for different values of mean velocity and

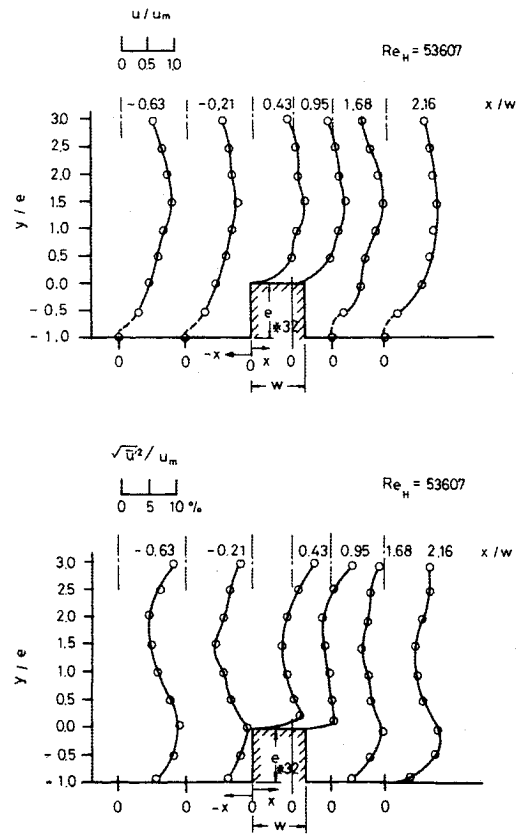

Fig. 11 Mean velocity and fluctuation intensity profiles for $Re_H = 53,607$ near a downstream rib.

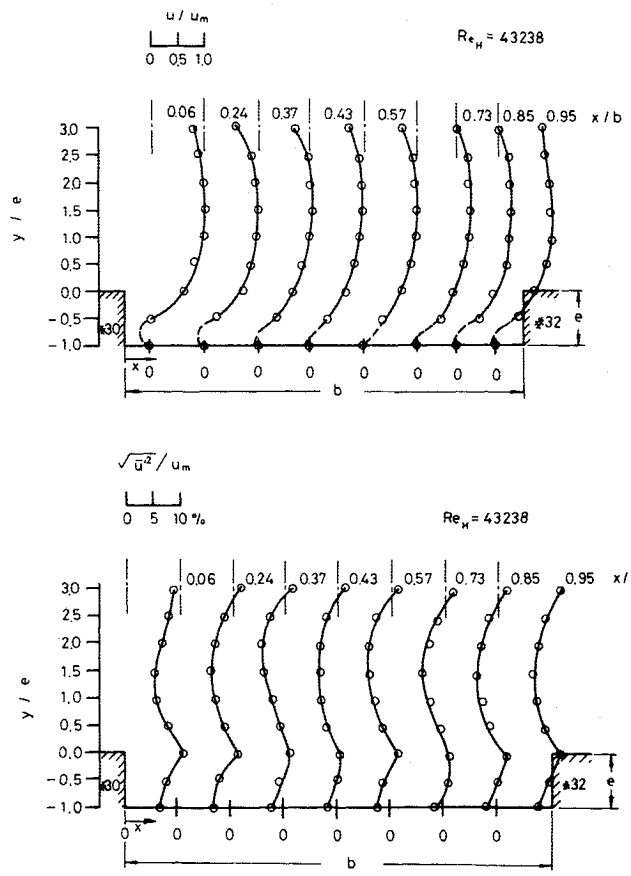

Fig. 12 Mean velocity and fluctuation intensity profiles for $Re_H = 43,238$ between two downstream consecutive ribs.

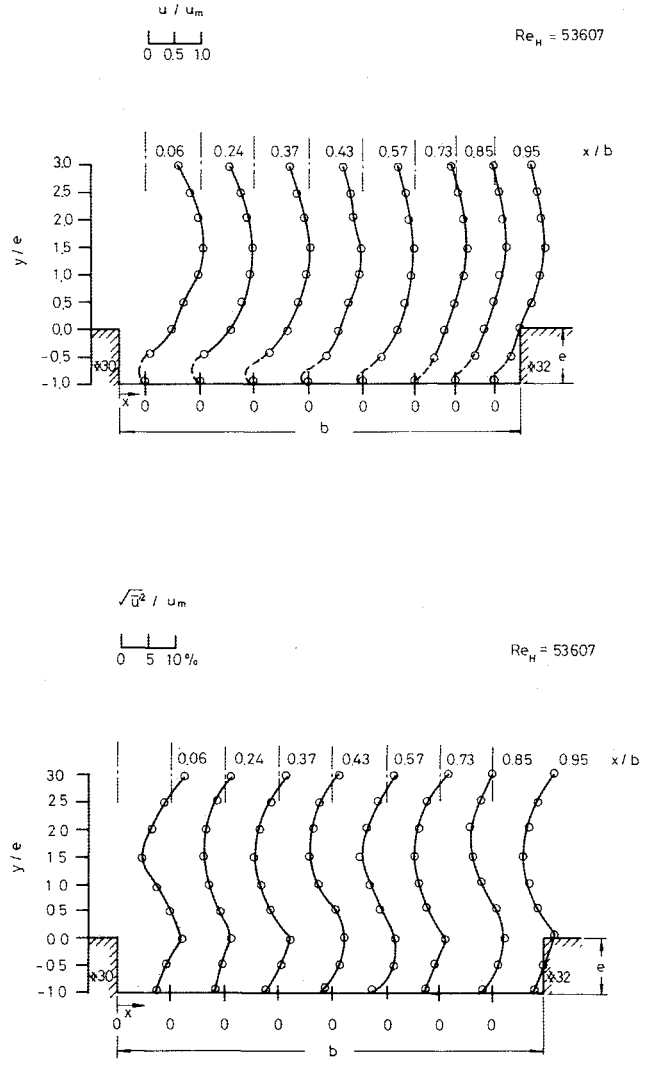

Fig. 13 Mean velocity and fluctuation intensity profiles for $Re_H = 53{,}607$ between two downstream consecutive ribs.

different maximum reverse velocities. For the valley of two consecutive ribs, the mean velocity profiles shown in Figs. 12a and 13a have features similar to these observed by Sinha et al.[22] However, the reattachment points and the maximum reverse velocities are different for different Reynolds numbers, as one would expect.

2) In general, in Figs. 10b, 11b, 12b, and 13b, turbulent intensity profiles at each downstream station show two maxima. The lower maximum near $y=0$ corresponds to the separating shear undergoing transition, the magnitude of u' increasing from about 5% to 10% for these two different test sections. The upper maximum were found where the maximum mean velocities were measured. The lower intensities measured were near the position between these two maxima. Thus, across the mainstream, the intensities decrease away from the rib until the center of the duct is nearly reached. The upper maximum in the core flow region as well as the lower one at each station seems consistent as the flow moves downstream, indicating the existence of the spatially periodic flow.

Conclusion

The nature of separating flow over separated ribs in a square duct with a definite staggered-type alignment ($p/e=5.31$, $e/D_H=0.19$) is investigated in the range of $100<Re_H<130{,}000$ to broaden our basic understanding of this type of flow. The most significant contributions of the present study are as follows.

1) The general flow pattern is quantitatively discussed through flow visualization technique.

2) Data on reattachment length (onset of separation length) for $100<Re_H<9000$ is found.

3) A streamwise periodic flow is approximately achieved after sufficient distance for development. An isothermal friction factor is obtained.

4) The intensity of fluctuation along with mean velocity profile was measured and discussed.

Further study may include the variation of the rib height and concentration to observe their effect on the flow pattern, reattachment length (onset of separation length), and turbulent intensity of this type of flow.

References

[1]Hsieh, S.-S. and Christensen, R. N., "Turbulent Heat Transfer on Rough Surface with Asymmetrical Heating," American Society of Mechanical Engineers, New York, ASME Paper 84-HT-54, Aug. 1984.

[2]Hsieh, S.-S., Liauh, C.-T., and Ku, A. C., "Thermal Analysis of the Performances of Helical-Type, Roughened, Double Pipe Heat Exchangers," *Applied Energy*, Vol. 26, Jan. 1987, pp. 67-73.

[3]Hsieh, S.-S., Liauh, C.-T., and Ku, A. C., "Heat Transfer Coefficient of Double Pipe Heat Exchanger with Helical Type Roughened Surface," *Journal of Heat Recovery System*, Vol. 7, April 1987, pp. 119-127.

[4]Hsieh, S.-S. and Huang, D.-Y., "Numerical Computation of Laminar Separated Forced Convection on Surface Mounted Ribs," *Numerical Heat Transfer*, Vol. 12, Nov. 1987, pp. 335-348.

[5]Hsieh, S.-S. and Huang, D.-Y., "Flow Characteristics of Laminar Separation on Surface-Mounted Ribs," *AIAA Journal*, Vol. 25, June 1987, pp. 819-824.

[6]Webb, R. L., Eckert, E. R. G., and Goldstein, R. J., "Heat Transfer and Friction in Tubes with Repeated-Rib Roughness," *International Journal of Heat and Mass Transfer*, Vol. 14, 1971, pp. 601-617.

[7]Hsieh, S.-S., "Thermal Characteristics of Annular Flow with Asymmetrically Roughened Surfaces," *International Journal of Heat and Fluid Flow*, Vol. 9, Jan. 1988, pp. 78-82.

[8]Nunner, W., "Heat Transfer and Pressure Drop in Rough Tubes," AERE lib/Trans. 786, 1958.

[9]Lewis, M. J., "An Elementary Analysis for Predicting the Momentum and Heat Transfer Characteristics of a Hydraulically Rough Surface," *Journal of Heat Transfer*, Vol. 97, 1975, pp. 249-254.

[10]Han, J. C., Glickman, L. R., and Rohsenow, W. M., "An Investigation of Heat Transfer and Friction for Rib-Roughened Surfaces," *International Journal of Heat and Mass Transfer*, Vol. 21, June 1980, pp. 1143-1156.

[11]Gee, D. L. and Webb, R. L., "Forced Convection Heat Transfer in Helically Rib-Roughened Tubes," *International Journal of Heat Transfer*, Vol. 23, May 1980, pp. 1127-1136.

[12]Suo, M., "Turbine Cooling," *The Aerothermodynamics of Aircraft Gas Turbine Engine*, edited by G. Oates, Air Force Aero Propulsion Lab., AFAPL TR-78-52, 1978.

[13]Taylor, J. R., "Heat Transfer Phenomena in Gas Turbine," American Society of Mechanical Engineers, New York, Paper 80-GT-172, 1980.

[14]Burggarff, F., "Experimental Heat Transfer and Pressure Drop with Two-Dimensional Turbulence Promoter Applied to Two Opposite Walls of a Square Tube," *Augmentation of Convective Heat and Mass Transfer*, edited by E. E. Bergles and R. L. Webb, American Society of Mechanical Engineers, New York, 1970, pp. 70-79.

[15]Han, J. C. and Lei, C. K., "Heat Transfer and Friction in Square Duct with Two Opposite Rib-Roughened Walls," American Society of Mechanical Engineers, New York, Paper 83-HT-26, 1983.

[16]Han, J. C., Park, J. S., and Lei, C. K., "Heat Transfer Enhancement in Channels with Turbulence Promoters," *Journal of Engineering for Gas Turbine and Power*, Vol. 107, July 1985, pp. 628-635.

[17]Islam, D. and Logan, E., "Channel Flow over Smooth-to-Rough Surface Discontinuity with Zero Pressure Gradient," *Journal of Fluids Engineering*, Vol. 98, No. 4, Dec. 1976, pp. 626-634.

[18]Perry, A. E., Schofield, W. H., and Joubert, P. H., "Rough Wall Turbulent Boundary Layers," *Jounal of Fluid Mechanics*, Vol. 37, Part II, May 1969, pp. 383-413.

[19]Savage, D. W. and Myers, J. E., "The Effects of Artificial Surface Roughness on Heat and Momentum Transfer," *American Institute of Chemical Engineers Journal*, Vol. 9, No. 5, Sept. 1963, pp. 694–702.

[20]Stukel, J. J., Hopke, P. K., and Nourmohammadi, K., "Turbulent Air Flow Over Rough Surfaces: Mean Flow Parameters," *Journal of Fluids Engineering*, Vol. 106, Dec. 1984, pp. 405–409.

[21]Nourmohammadi, K., Hopke, P. K., and Stukel, J. J., "Turbulent Air Flow Over Rough Surfaces: Turbulent Flow Parameters," *Journal of Fluids Engineering*, Vol. 107, March 1985, pp. 55–60.

[22]Sinha, S. N., Gupta, A. K., and Oberai, M. M., "Laminar Separating Flow Over Backsteps and Cavities, Part II: Cavities," *AIAA Journal*, Vol. 20, March 1982, pp. 370–375.

[23]Tritton, D. J., "Experiments on the Flow Past a Circular Cylinder at Low Reynolds Number," *Journal of Fluid Mechanics*, Vol. 6, Nov. 1959, pp. 547–567.

[24]Kline, S. J. and McClintock, F. A., "The Description of Uncertainties in Single Sample Experiments," *Mechanical Engineering*, Vol. 75, Jan. 1953, pp. 3–8.

[25]Benodekar, R. W., Goddard, A. J. H., Gosman, A. D., and Issa, R. I., "Numerical Prediction of Turbulent Flow over Surface-Mounted Ribs, "*AIAA Journal*, Vol. 23, March 1985, pp. 359–366.